Rare Semileptonic B_s Decays to η and η' mesons in QCD

K. Azizi[1] *, R. Khosravi[2] †, F. Falahati[2] ‡

[1] *Physics Division, Faculty of Arts and Sciences,*

Doğuş University, Acıbadem-Kadıköy, 34722 Istanbul, Turkey

[2] *Physics Department, Shiraz University, Shiraz 71454, Iran*

Abstract

We analyze the rare semileptonic $B_s \to (\eta, \eta')l^+l^-$, $(l = e, \mu, \tau)$ and $B_s \to (\eta, \eta')\nu\bar{\nu}$ transitions probing the $\bar{s}s$ content of the η and η' mesons via three–point QCD sum rules. We calculate responsible form factors for these transitions in full theory. Using the obtained form factors, we also estimate the related branching fractions and longitudinal lepton polarization asymmetries. Our results are in a good consistency with the predictions of the other existing nonperturbative approaches.

PACS numbers: 11.55.Hx, 13.20.He

* e-mail: kazizi @ dogus.edu.tr

† e-mail: khosravi.reza @ gmail.com

‡ e-mail: falahati@shirazu.ac.ir

I. INTRODUCTION

Among B mesons, the B_s has been received special attention, since experimentally it is expected that an abundant number of B_s will be produced at LHCb. This will provide possibility to study properties of the this meson and its various decay channels. The first evidence for B_s production at the $\Upsilon(5S)$ peak was found by the CLEO collaboration [1, 2]. Recently, the Belle Collaboration measured the branching ratios of the $B_s \to J/\psi\phi$ transition as well as the $B_s \to J/\psi\eta$ decay via the $\eta \to \gamma\gamma$ and $\eta \to \pi^+\pi^0\pi^-$ channels to reconstruct the η meson [3].

Semileptonic decays of the B_s to the η and η', induced by the rare flavor changing neutral current (FCNC) transition of $b \to sl^+l^-$ and $b \to s\nu\bar{\nu}$ are crucial framework to restrict the SM parameters. They can provide possibility to extract the elements of the Cabbibo-Kobayashi-Maskawa (CKM) matrix and search for origin of the CP and T violations. As these transitions occur at the lowest order through one-loop penguin diagrams, they are good context to search for new physics effects beyond the SM. Looking for supersymmetric particles [4], light dark matter [5] and fourth generation of quarks is possible via these transitions. These transitions are also useful to study structures of the η and η' mesons.

In the present work, we analyze the semileptonic $B_s \to (\eta, \eta')l^+l^-/\nu\bar{\nu}$ decays considering also the $\bar{s}s$ content of the η and η' mesons in the framework of the three point QCD sum rules. Here, we consider also the mixing between the η and η' states with a single mixing angle [6, 7] as:

$$\begin{aligned} |\eta\rangle &= \cos\varphi|\eta_q\rangle - \sin\varphi|\eta_s\rangle \\ |\eta'\rangle &= \sin\varphi|\eta_q\rangle + \cos\varphi|\eta_s\rangle \quad . \end{aligned} \tag{1}$$

where, in the quark favor (QF) basis (for more details see for instance [8, 9]),

$$\begin{aligned} |\eta_q\rangle &= \frac{1}{\sqrt{2}}\left(|\bar{u}u\rangle + |\bar{d}d\rangle\right), \\ |\eta_s\rangle &= |\bar{s}s\rangle \ . \end{aligned} \tag{2}$$

The decay constants of $\bar{q}q$ and $\bar{s}s$ parts are defined in terms of the pion decay constant as [6]:

$$f_q = (1.02 \pm 0.02)f_\pi, \qquad f_s = (1.34 \pm 0.06)f_\pi. \tag{3}$$

We will use the mixing angle $\varphi = (41.5 \pm 0.3_{stat} \pm 0.7_{syst} \pm 0.6_{th})^{\circ}$ [10], which has recently been obtained by the KLOE Collaboration in QF basis via measuring the ratio $\frac{\Gamma(\phi \to \eta'\gamma)}{\Gamma(\phi \to \eta\gamma)}$. In the QF basis with the single mixing angle, the form factors of $B_s \to \eta(\eta')$ transitions are defined in terms of the form factors $B_s \to \eta_s$ as:

$$f_i^{B_s \to \eta(\eta')} = -\sin\varphi\,(\cos\varphi)\, f_i^{B_s \to \eta_s}, \tag{4}$$

and their branching fractions are also related to the branching ratio of $B_s \to \eta_s$ as follows:

$$\mathrm{BR}\left\{B_s \to \eta(\eta') l^+ l^-\right\} = \sin^2\varphi\left(\cos^2\varphi\right)\mathrm{BR}\left\{B_s \to \eta_s l^+ l^-\right\}. \tag{5}$$

The paper is organized as follows: sum rules for form factors responsible for considered transitions are obtained in Section II. Section III is devoted to the numerical analysis of the form factors, branching ratios and longitudinal lepton polarization asymmetries as well as our discussions. In this section, we also compare the obtained results with the existing predictions of the other non-perturbative approaches.

II. QCD SUM RULES FOR TRANSITION FORM FACTORS

As we previously mentioned, to calculate the form factors responsible for the rare semileptonic $B_s \to (\eta, \eta') l^+ l^-$, $(l = e, \mu, \tau)$ and $B_s \to (\eta, \eta')\nu\bar{\nu}$ decays, we need to calculate the form factors of $B_s \to \eta_s l^+ l^- / \nu\bar{\nu}$. For this aim, we start with the following three-point correlation function, which is constructed from the vacuum expectation value of time ordered product $\mathcal{T}$ of interpolating fields of initial and final mesons and transition currents, J^V and J^T, as follow:

$$\Pi_\mu^{V,T} = i^2 \int d^4x d^4y e^{-ipx} e^{ip'y} \langle 0|\mathcal{T}\left\{J_5^s(y) J_\mu^{V,T}(0) J_{B_s}^\dagger(x)\right\}|0\rangle\ , \tag{6}$$

where p and p' are initial and final momentums, respectively, $J_{B_s}(x) = \bar{s}(x)\gamma_5 b(x)$ and $J_5^s(y) = \bar{s}(y)\gamma_5 s(y)$, are the interpolating currents of the B_s and η_s states and $J_\mu^V(0) = \bar{s}(0)\gamma_\mu b(0)$ and $J_\mu^T(0) = \bar{s}(0)\sigma_{\mu\nu}q^\nu b(0)$ are the vector and tensor transition currents extracted from the effective Hamiltonian responsible for $B_s \to \eta_s l^+ l^- / \nu\bar{\nu}$ decays. At quark level, these transitions are governed by $b \to s l^+ l^-$ and $b \to s\nu\bar{\nu}$ via penguin and box diagrams (see Fig. (1)). The corresponding effective Hamiltonian is presented in terms of the Wilson coefficients, C_7^{eff}, C_9^{eff} and C_{10} as:

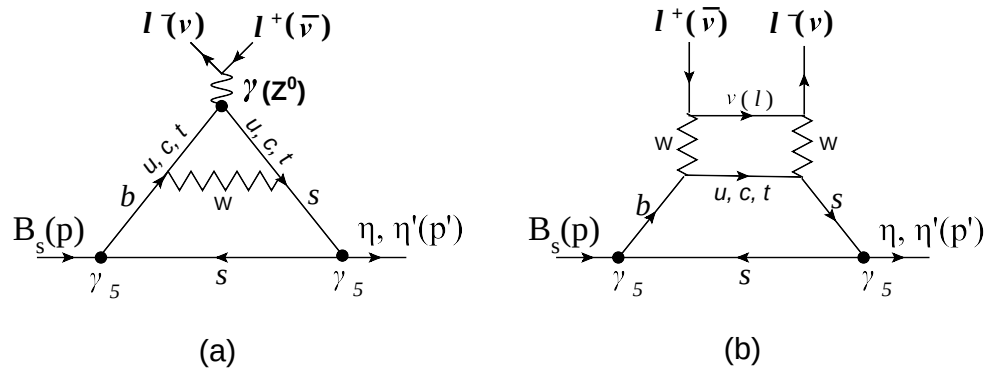

FIG. 1: Diagrams responsible for the $B_s \to (\eta, \eta')l^+l^-/\nu\bar{\nu}$ transitions.

$$\mathcal{H}_{eff} = \frac{G_F\alpha}{2\sqrt{2}\pi} V_{tb}V_{ts}^* \Big[C_9^{eff}\, \bar{s}\gamma_\mu(1-\gamma_5)b\, \bar{\ell}\gamma_\mu\ell + C_{10}\, \bar{s}\gamma_\mu(1-\gamma_5)b\, \bar{\ell}\gamma_\mu\gamma_5\ell - 2C_7^{eff}\frac{m_b}{q^2}\, \bar{s}\, i\sigma_{\mu\nu}q^\nu(1+\gamma_5)b\, \bar{\ell}\gamma_\mu\ell \Big] , \tag{7}$$

where G_F is the Fermi constant, α is the fine structure constant at Z mass scale, and V_{ij} are elements of the CKM matrix. For $\nu\bar{\nu}$ case, only the term containing C_{10} is considered. It should be mentioned that because of the parity conservations, the axial vector and pseudotensor currents do not contribute to the pseudoscalar–pseudoscalar hadronic matrix element, i.e.,

$$\begin{aligned} \langle P(p') \mid J_\mu^{AV} &= \bar{s}\gamma_\mu\gamma_5 b \mid B_s(p)\rangle = 0 \ , \\ \langle P(p') \mid J_\mu^{PT} &= \bar{s}\ i\sigma_{\mu\nu}q^\nu\gamma_5 b \mid B_s(p)\rangle = 0 \ , \end{aligned} \tag{8}$$

where, P stands for $\eta(\eta')$ meson.

From the general aspect of the QCD sum rules, we calculate the aforementioned correlation function in two different ways. First, in the hadronic representation, it is calculated in time-like region in terms of hadronic parameters called phenomenological or physical side. Second, it is calculated in space-like region in terms of QCD degrees of freedom called the QCD or theoretical side. The sum rules for the form factors can be obtained equating the coefficient of the selected structures from these two representations of the same correlation function through dispersion relation and applying double Borel transformation with respect to the momentums of the initial and final states to suppress the contributions coming from the higher states and continuum.

In order to obtain the phenomenological representation of the correlation function given in Eq. (6), two complete sets of intermediate states with the same quantum numbers as the interpolating currents J_{η_s} and J_{B_s} are inserted to sufficient places. As a result of this procedure, we obtain,

$$\Pi_\mu^{V,T}(p^2,p'^2,q^2) = \frac{\langle 0 \mid J_5^s \mid P(p')\rangle\langle P(p') \mid J_\mu^{V,T} \mid B_s(p)\rangle\langle B_s(p) \mid J_{B_s}^\dagger \mid 0\rangle}{(p'^2-m_P^2)(p^2-m_{B_s}^2)} + \cdots \tag{9}$$

where $\cdots$ represents the contributions coming from the higher states and continuum. The following matrix elements $\langle 0|J_{B_s}|P\rangle$ and $\langle 0|J_5^s|P\rangle$ are defined in terms of the leptonic decay constant and four parameters h_P^s as:

$$\begin{aligned}\langle 0|J_{B_s}|B_s\rangle &= -i\frac{f_{B_s}m_{B_s}^2}{m_b+m_s}\ ,\\ \langle 0|J_5^s|P\rangle &= -i\frac{h_P^s}{2m_s}\ .\end{aligned} \tag{10}$$

where correlating the h_P^s to f_s and f_q, the values $h_\eta^s = -0.053\ GeV^3$ and $h_{\eta'}^s = 0.065\ GeV^3$ are obtained (for details see [6]). From Lorentz invariance and parity considerations, the remaining matrix element, i.e., transition matrix element in Eq. (9) is parameterized in terms of form factors in the following way:

$$\begin{aligned}\langle P(p') \mid J_\mu^V \mid B_s(p)\rangle &= \mathcal{P}_\mu f_+(q^2) + q_\mu f_-(q^2)\ ,\\ \langle P(p') \mid J_\mu^T \mid B_s(p)\rangle &= \frac{f_T(q^2)}{m_{B_s}+m_P}\Big[\mathcal{P}_\mu q^2 - q_\mu(m_{B_s}^2-m_P^2)\Big]\ ,\end{aligned} \tag{11}$$

where, $f_+(q^2), f_-(q^2)$ and $f_T(q^2)$ are the transition form factors, which only depend on the momentum transfer squared q^2, $\mathcal{P}_\mu = (p+p')_\mu$ and $q_\mu = (p-p')_\mu$.

Using Eqs. (10) and (11) in Eq. (9), we obtain

$$\begin{aligned}\Pi_\mu^V(p^2,p'^2,q^2) &= \frac{f_{B_s}m_{B_s}^2}{2m_s(m_b+m_s)}\frac{h_P^s}{(m_P^2-p'^2)(m_{B_s}^2-p^2)}\Big[f_+(q^2)\mathcal{P}_\mu + f_-(q^2)q_\mu\Big],\\ \Pi_\mu^T(p^2,p'^2,q^2) &= \frac{f_{B_s}m_{B_s}^2}{2m_s(m_b+m_s)}\frac{h_P^s}{(m_P^2-p'^2)(m_{B_s}^2-p^2)}\Bigg[\frac{f_T(q^2)}{(m_{B_s}+m_P)}\\ &\times \Big(q^2\mathcal{P}_\mu - (m_{B_s}^2-m_P^2)q_\mu\Big)\Bigg].\end{aligned} \tag{12}$$

For extracting the sum rules for form factors $f_+(q^2)$ and $f_-(q^2)$, we choose the coefficients of the structures $\mathcal{P}_\mu$ and q_μ from $\Pi_\mu^V(p^2,p'^2,q^2)$, respectively and the structure q_μ from $\Pi_\mu^T(p^2,p'^2,q^2)$ is considered to calculate the form factor $f_T(q^2)$. Therefore, the correlation

functions are written in terms of the selected structures as:

$$\Pi^V_\mu(p^2,p'^2,q^2)=\Pi_+\mathcal{P}_\mu+\Pi_-q_\mu \ ,$$
$$\Pi^T_\mu(p^2,p'^2,q^2)=\Pi_Tq_\mu \ . \tag{13}$$

Now, we focus our attention to calculate the to calculate the QCD side of the correlation function. This side is calculated at deep Euclidean space, where $-p^2\to\infty$ and $-p^{'2}\to\infty$ via operator product expansion (OPE). For this aim, we write each Π_i function (coefficient of each structure) in terms of the perturbative and non–perturbative parts as:

$$\Pi_i=\Pi_i^{per}+\Pi_i^{non-per} \ , \tag{14}$$

where i stands for $+$, $-$ and T. The perturbative part is written in terms of double dispersion integral as:

$$\Pi_i^{per}=-\frac{1}{(2\pi)^2}\int ds'\int ds\frac{\rho_i^{per}(s,s',q^2)}{(s-p^2)(s'-p'^2)}+\text{subtraction terms} \ , \tag{15}$$

where, the $\rho_i^{per}(s,s',q^2)$ are called spectral densities. To get the spectral densities, we need to evaluate the bare loop diagrams in Fig. (1). Calculating these diagrams via the usual Feynman integrals with the help of the Cutkosky rules, i.e. $\frac{1}{p^2-m^2}\to-2\pi\delta(p^2-m^2)$, which implies that all quarks are real, leads to the following spectral densities:

$$\begin{aligned}
\rho_+^{per}(s,s',q^2) &= I_0N_c\{\Delta+s'-2m_s^2+2m_bm_s+(E_1+E_2)u\} \ ,\\
\rho_-^{per}(s,s',q^2) &= I_0N_c\{-\Delta+s'+2m_s^2-2m_bm_s+(E_1-E_2)u\} \ ,\\
\rho_T^{per}(s,s',q^2) &= -I_0N_c\{\Delta(m_b-m_s)+s'(m_s-m_b)+2m_ss+2[m_b(E_1-E_2)\\
&\quad +m_s(E_2-E_1-1)]s'+(E_1-E_2)(m_s-m_b)u\} \ ,
\end{aligned} \tag{16}$$

where

$$\begin{aligned}
I_0(s,s',q^2) &= \frac{1}{4\lambda^{1/2}(s,s',q^2)} \ ,\\
\lambda(s,s',q^2) &= s^2+s'^2+q^4-2sq^2-2s'q^2-2ss' \ ,\\
E_1 &= \frac{1}{\lambda(s,s',q^2)}[2s'\Delta-s'u] \ ,\\
E_2 &= \frac{1}{\lambda(s,s',q^2)}[2ss'-\Delta u] \ ,\\
u &= s+s'-q^2 \ ,\\
\Delta &= s+m_s^2-m_b^2 \ ,
\end{aligned} \tag{17}$$

and $N_c = 3$ is the color factor.

For calculation of non–perturbative contributions in QCD side, the condensate terms of OPE are considered. The condensate term of dimension 3 is related to contribution of quark condensate. Fig .(2) shows quark–quark condensate diagrams of dimension 3. It should be reminded that the quark condensate are considered only for light quarks and the heavy quark condensate is suppressed by inverse powers of the heavy quark mass. The

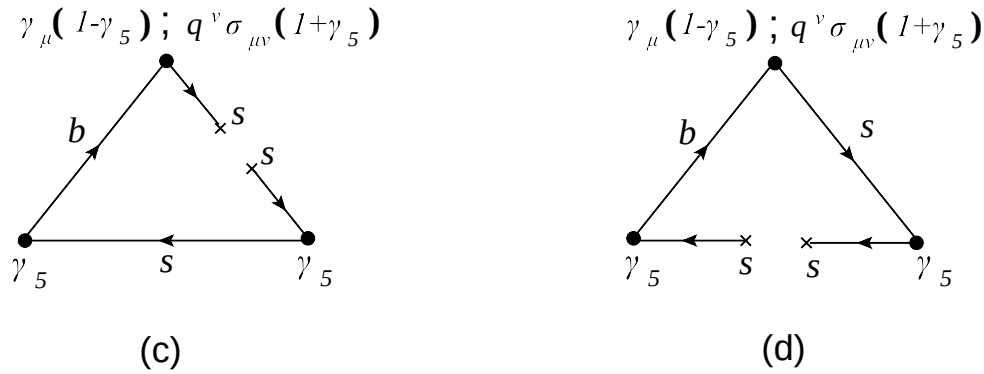

FIG. 2: Quark–quark condensate diagrams.

contribution of the diagram (c) in Fig .(2) is zero since applying double Borel transformation with respect to the both variables p^2 and p'^2 kills its contribution, because only one variable appears in the denominator in this case. Therefore as dimension 3, we consider only diagram (d) in Fig .(2). The dimension 4 operator in OPE is the gluon–gluon condensate. Our calculations show that in this case, the gluon–gluon condensate contributions are very small in comparison with the quark–quark and quark-gluon condensates contributions and we can easily ignore their contributions. The next operator is dimension 5 quark–gluon condensate. The diagrams corresponding to quark–gluon condensate are presented in Fig. (3). Contributions of the diagrams (e) and (f) vanish with the same reason as for diagram (c) in Fig .(2). Therefore, only diagrams (g) and (h) contribute to the non–perturbative part of dimension 5. In QCD sum rule approach, the OPE is truncated at some finite order such that Borel transformations play an important role in this cutting. Mainly, the proper regions of the Borel parameters are adopted by demanding that in the truncated OPE, the condensate term with the highest dimension constitutes a small fraction of the total dispersion integral. In the next section, we will explain how these proper regions are obtained. Hence, we will not consider the condensates with $d \geq 6$ that play a minor role in our calculations.

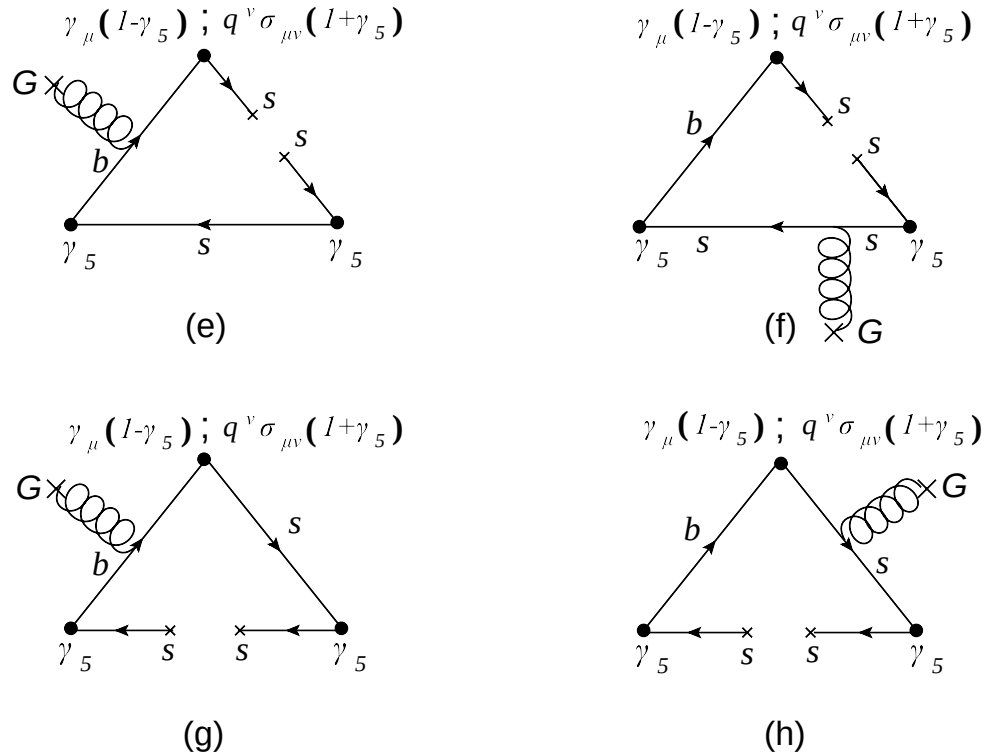

FIG. 3: Quark–gluon condensate diagrams.

The explicit expressions of $\Pi_i^{non-per}$, are given in the Appendix–A.

The next step is to apply the double Borel transformations with respect to the $p^2(p^2 \to M_1^2)$ and $p'^2(p'^2 \to M_2^2)$ on the phenomenological as well as the perturbative and non–perturbative parts of the QCD side and equate the two representations. As a result, the following sum rules for the form factors are derived:

$$f_i'(q^2)=\frac{(m_b+m_s)(2m_s)}{f_{B_s}m_{B_s}^2 h_P^s}e^{m_{B_s}^2/M_1^2}e^{m_P^2/M_2^2} \times\left\{-\frac{1}{4\pi^2}\int_{2m_s^2}^{s_0'}ds'\int_{s_L}^{s_0}ds\rho_i^{per}(s,s',q^2)e^{-s/M_1^2}e^{-s'/M_2^2}+\tilde{B}\Pi_i^{non-per}(p^2,p'^2,q^2)\right\}, \tag{18}$$

where, $f_+'(q^2)=f_+(q^2)$, $f_-'(q^2)=f_-(q^2)$ and $f_T'(q^2)=-f_T(q^2)(m_{B_s}-m_P)$. The s_0 and s_0' are the continuum thresholds in initial and final channels, respectively and s_L is the lower limit of the integral over s. It is obtained as:

$$s_L=\frac{(m_s^2+q^2-m_b^2-s')(m_b^2s'-q^2m_s^2)}{(m_b^2-q^2)(m_s^2-s')}\ . \tag{19}$$

Also the operator $\tilde{B}$ in Eq. (18) is defined as:

$$\tilde{B} = \mathcal{B}_{p^2}(M_1^2)\mathcal{B}_{p'^2}(M_2^2) \ , \tag{20}$$

where, M_1^2 and M_2^2 are Borel mass parameters. It should be also noted that to subtract the contributions of the higher states and the continuum the quark–hadron duality assumption is also used,

$$\rho^{higherstates}(s,s') = \rho^{OPE}(s,s')\theta(s-s_0)\theta(s'-s_0') \ . \tag{21}$$

III. NUMERICAL ANALYSIS

We are now ready to present our numerical analysis of the form factors $f_+(q^2)$, $f_-(q^2)$ and $f_T(q^2)$ and calculate branching fractions and longitudinal lepton polarization asymmetries. In our numerical calculations, we use the following values for input parameters: $m_s = 0.13\ GeV$, $m_b = 4.8\ GeV$, $m_\eta = (547.51 \pm 0.18)\ MeV$, $m_{\eta'} = (957.78 \pm 0.14)\ MeV$, $m_{B_s} = (5366.3 \pm 0.6)\ MeV$ [11], $|V_{tb}V_{ts}^*| = 0.0385$, $C_7^{eff} = -0.313$, $C_9 = 4.344$, $C_{10} = -4.669$ [12], $f_{B_s} = (209 \pm 38)\ MeV$ [13], $m_0^2 = (0.8 \pm 0.2)\ GeV^2$, $\langle s\bar{s}\rangle = (0.8 \pm 0.2)\langle u\bar{u}\rangle$ and $\langle u\bar{u}\rangle = -(0.240 \pm 0.010)^3\ GeV^3$.

The sum rules for the form factors contain also four auxiliary parameters, namely Borel mass squares, M_1^2 and M_2^2 and continuum thresholds, s_0 and s_0. These are not physical quantities, so our results should be independent of them. The parameters s_0 and s_0' are not totally arbitrary but they are related to the energy of the first excited stateS with the same quantum numbers as the interpolating currents. They are determined from the conditions that guarantee the sum rules to have the best stability in the allowed M_1^2 and M_2^2 regions. The value of continuum threshold s_0 calculated from the two–point QCD sum rules are taken to be $s_0 = (34.2 \pm 2)\ GeV^2$ [14]. We use also the range, $(m_P + 0.3)^2 \leq s_0' \leq (m_P + 0.5)^2\ GeV^2$ in $P = \eta(\eta')$ channel. The working regions for M_1^2 and M_2^2 are determined demanding that not only the contributions of the higher states and continuum are effectively suppressed, but contributions of the higher dimensional operators are also small. Both conditions are satisfied in the regions, $12\ GeV^2 \leq M_1^2 \leq 22\ GeV^2$ and $4\ GeV^2 \leq M_2^2 \leq 10\ GeV^2$.

The dependence of the form factors f_+, f_- and f_T on M_1^2 and M_2^2 for $B_s \to \eta_s$ transition when $m_P = m_\eta$ are shown in Fig. 4. The Fig. 5, also depicts the dependence of the same

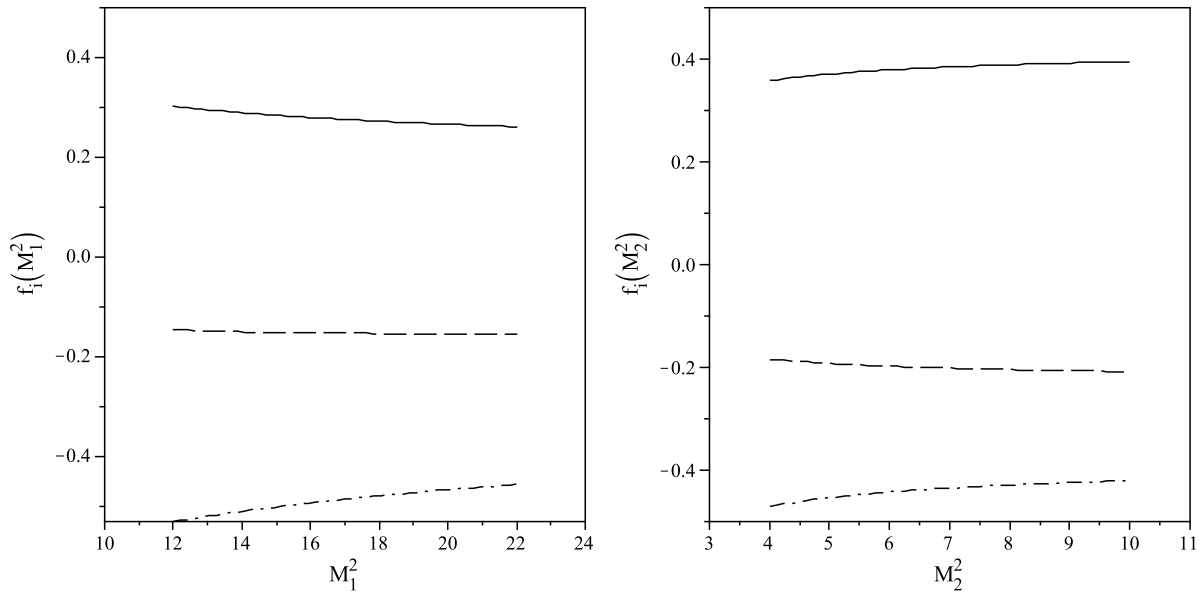

FIG. 4: The dependence of the form factors on M_1^2 and M_2^2 for $B_s \to \eta_s$ decay when $m_P = m_\eta$. The solid, dashed and dashed-dotted lines correspond to the f_+, f_- and f_T, respectively.

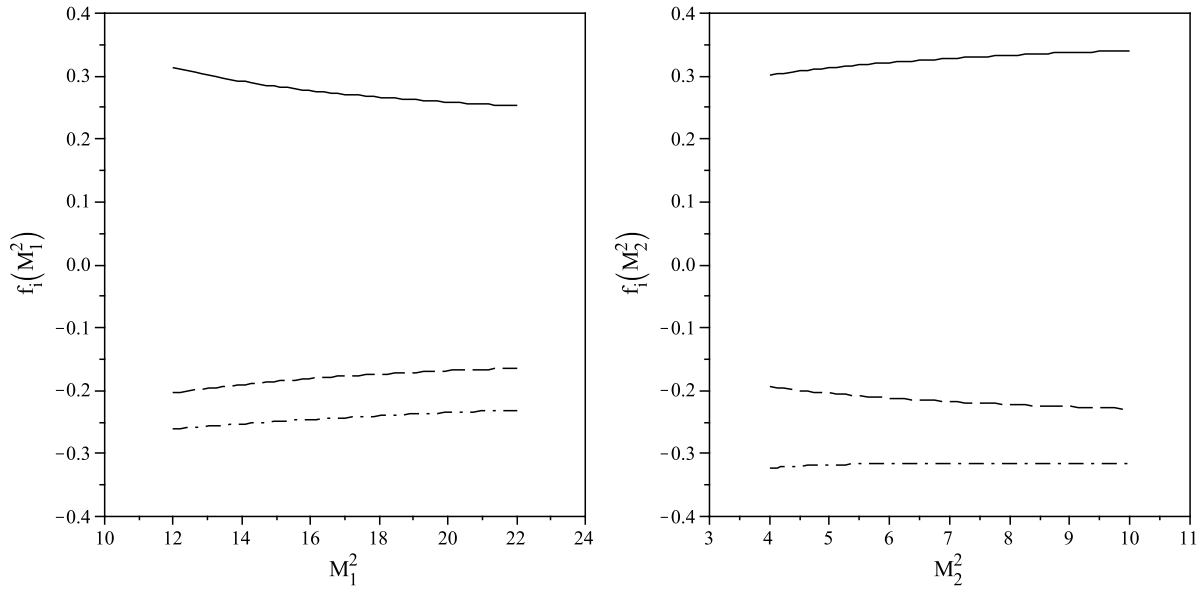

FIG. 5: The dependence of the form factors on M_1^2 and M_2^2 for $B_s \to \eta_s$ decay when $m_P = m_{\eta'}$. The solid, dashed and dashed-dotted lines correspond to the f_+, f_- and f_T, respectively.

form factors on Borel mass parameters for $B_s \to \eta_s$ decay when $m_P = m_{\eta'}$. These figures show a good stability of the form factors with respect to the Borel mass parameters in the working regions. Using these regions for M_1^2 and M_2^2, our numerical analysis shows that the contribution of the non–perturbative part to the QCD side is about 21% of the total

and the main contribution comes from the perturbative part.

Now, we proceed to present the q^2 dependency of the form factors. Since the form factors $f_\pm(q^2)$ and $f_T(q^2)$ are calculated in the space-like ($q^2 < 0$) region, we should analytically continue them to the time-like ($q^2 > 0$) or physical region. Hence, we should change q^2 to $-q^2$. As we previously mentioned, the form factors are truncated at approximately, 1 GeV below the perturbative cut. Therefore, to extend our results to the full physical region, we look for parametrization of the form factors in such a way that in the reliable region the results of the parametrization coincide with the sum rules predictions. Our numerical calculations show that the sufficient parametrization of the form factors with respect to q^2 is:

$$f_i(q^2) = \frac{f_i(0)}{1 + \alpha\hat{q} + \beta\hat{q}^2} \ , \tag{22}$$

where $\hat{q} = q^2/m_{B_s}^2$. The values of the parameters $f_i(0)$, α and β are given in the Table I taking $M_1^2 = 12\ GeV^2$ and $M_2^2 = 5\ GeV^2$. This Table also contains the predictions of the light-front quark model (LFQM).

$B_s \to \eta_s(P=\eta)$			$B_s \to \eta_s(P=\eta')$		
Parameters	This work	LFQM[8]	Parameters	This work	LFQM[8]
$f_+(0)$	0.364 ± 0.120	0.291	$f_+(0)$	0.337 ± 0.111	0.291
α	-0.333 ± 0.107	-1.574	α	-0.495 ± 0.158	-1.575
β	-0.694 ± 0.222	0.751	β	-0.820 ± 0.262	0.770
$f_-(0)$	-0.189 ± 0.062	-0.231	$f_-(0)$	-0.193 ± 0.064	-0.225
α	-0.833 ± 0.267	-1.582	α	-1.028 ± 0.329	-1.570
β	-0.168 ± 0.054	0.825	β	-0.048 ± 0.015	0.835
$f_T(0)$	-0.444 ± 0.147	-0.280	$f_T(0)$	-0.424 ± 0.140	-0.300
α	-0.453 ± 0.145	-1.561	α	-0.596 ± 0.191	-1.561
β	-0.355 ± 0.114	0.782	β	-0.381 ± 0.122	0.802

TABLE I: Parameters appearing in the fit function for form factors of $B_s \to \eta_s$ in two approaches.

The values of the form factors at $q^2 = 0$ are also compared with the predictions of the other nonperturbative approaches such as, LFQM and constituent quark model (CQM) in Table II. The dependence of the form factors $f_+(q^2)$, $f_-(q^2)$ and $f_T(q^2)$ on q^2 extracted

Mode	Form factors	This work	LFQM[8]	LFQM[16]	CQM [16]
	$f_+(0)$	0.364 ± 0.120	0.291	0.354	0.357
$B_s \to \eta_s(P=\eta)$	$f_-(0)$	-0.189 ± 0.062	-0.231	-0.360	-0.304
	$f_T(0)$	-0.444 ± 0.147	-0.280	-0.369	-0.365
	$f_+(0)$	0.337 ± 0.111	0.291	0.354	0.357
$B_s \to \eta_s(P=\eta')$	$f_-(0)$	-0.193 ± 0.064	-0.225	-0.324	-0.304
	$f_T(0)$	-0.424 ± 0.140	-0.300	-0.404	-0.390

TABLE II: The form factors of the $B_s \to \eta_s$ decay for $M_1^2 = 12\ GeV^2$ and $M_2^2 = 5\ GeV^2$ at $q^2 = 0$ in different approaches: this work (3PSR), light-front quark model (LFQM) and constituent quark model (CQM).

from the fit function are given in Figs. (6) and (7) for the $P = \eta$ and $P = \eta'$ cases, respectively. These figures also contain the values of form factors obtained directly from our sum rules in reliable region. These values coincide well with the values obtained from the fit function below the perturbative cut. Therefore, the aforementioned fit parametrization better describe our form factors. The form factors of $B_s \to \eta$ and $B_s \to \eta'$ are obtained using values in Table I and also Eq. (4).

Now, we would like to evaluate the branching ratios for the considered decays. Using the parametrization of these transitions in terms of the form factors, we get [15]:

$$\begin{aligned}
\frac{d\Gamma}{dq^2}(B_s \to P\nu\bar{\nu}) &= \frac{A\ G_F^2 |V_{ts}V_{tb}^*|^2 m_{B_s}^3 \alpha^2}{2^8\pi^5}\ \frac{|D_\nu(x_t)|^2}{sin^4\theta_W}\ \phi^{3/2}(1,\hat{r},\hat{s})|f_+(q^2)|^2\ , \\
\frac{d\Gamma}{dq^2}\left(B_s \to Pl^+l^-\right) &= \frac{A\ G_F^2 |V_{ts}V_{tb}^*|^2 m_{B_s}^3 \alpha^2}{3\cdot 2^9\pi^5} v\phi^{1/2}(1,\hat{r},\hat{s})\left[\left(1+\frac{2\hat{l}}{\hat{s}}\right)\phi(1,\hat{r},\hat{s})\alpha_1 + 12\ \hat{l}\beta_1\right]\ ,
\end{aligned} \tag{23}$$

where $A = \sin^2\varphi$ for $B_s \to \eta$ and $A = \cos^2\varphi$ for $B_s \to \eta'$ transitions. The $\hat{r}$, $\hat{s}$, $\hat{l}$, x_t and $\hat{m}_b$ and the functions v, $\phi(1,\hat{r},\hat{s})$, $D_\nu(x_t)$, α_1 and β_1 are defined as:

$$\begin{aligned}
\hat{r} &= \frac{m_P^2}{m_{B_s}^2}\ , \quad \hat{s} = \frac{q^2}{m_{B_s}^2}\ , \quad \hat{l} = \frac{m_l^2}{m_{B_s}^2}\ , \quad x_t = \frac{m_t^2}{m_W^2}\ , \quad \hat{m}_b = \frac{m_b}{m_{B_s}}\ , \\
v &= \sqrt{1-\frac{4\hat{l}}{\hat{s}}}\ ,
\end{aligned}$$

$$
\begin{aligned}
\phi(1,\hat{r},\hat{s}) &= 1+\hat{r}^2+\hat{s}^2-2\hat{r}-2\hat{s}-2\hat{r}\hat{s}\ , \\
D_\nu(x_t) &= \frac{x_t}{8}\left(\frac{2+x_t}{x_t-1}+\frac{3x_t-6}{(x_t-1)^2}\ln x_t\right)\ , \\
\alpha_1 &= \left|C_9^{\rm eff}\, f_+(q^2)+\frac{2\,\hat{m}_b\, C_7^{\rm eff}\, f_T(q^2)}{1+\sqrt{\hat{r}}}\right|^2+|C_{10}f_+(q^2)|^2\ , \\
\beta_1 &= |C_{10}|^2\left[\left(1+\hat{r}-\frac{\hat{s}}{2}\right)|f_+(q^2)|^2+\left(1-\hat{r}\right)\mathrm{Re}(f_+(q^2)f_-^*(q^2))+\frac{1}{2}\hat{s}|f_-(q^2)|^2\right].
\end{aligned}
\tag{24}
$$

Integrating Eq. (23) over q^2 in the whole physical region and using the total mean lifetime $\tau_{B_s}=(1.466\pm0.059)\ ps$ [11], the branching ratios of the $B_s\to(\eta,\eta')l^+l^-/\nu\bar{\nu}$ are obtained as presented in Table III. In this Table, we show only the values obtained considering the

Mode	This work	LFQM[8]	LFQM[16]	CQM[16]	set A[9]	set B[9]	set C[9]
$Br(B_s\to\eta\nu\bar{\nu})\times10^6$	1.35 ± 0.56	1.54	2.56(2.34)	2.38(2.17)	0.95 ± 0.2	2.2 ± 0.7	2.9 ± 1.5
$Br(B_s\to\eta'\nu\bar{\nu})\times10^6$	1.33 ± 0.55	1.47	2.36(2.52)	2.23(2.38)	0.9 ± 0.2	1.9 ± 0.5	2.4 ± 1.3
$Br(B_s\to\eta\mu^+\mu^-)\times10^7$	2.30 ± 0.97	2.09	3.75(3.42)	3.42(3.12)	1.2 ± 0.3	2.6 ± 0.7	3.4 ± 1.8
$Br(B_s\to\eta'\mu^+\mu^-)\times10^7$	2.24 ± 0.94	1.98	3.40(3.63)	3.19(3.41)	1.1 ± 0.3	2.2 ± 0.6	2.8 ± 1.5
$Br(B_s\to\eta\tau^+\tau^-)\times10^8$	3.73 ± 1.56	5.14	7.33(6.70)	7.33(6.70)	3 ± 0.5	8 ± 1.5	10 ± 5.5
$Br(B_s\to\eta'\tau^+\tau^-)\times10^8$	2.80 ± 1.18	2.86	4.66(5.00)	4.04(4.30)	1.55 ± 0.3	3.85 ± 0.75	4.7 ± 2.5

TABLE III: The branching ratios in different models corresponding to $\varphi=41.5^\circ$. The values in parentheses related to $\varphi=39.3^\circ$.

short distance (SD) effects contributing to the Wilson coefficient $C_9^{\rm eff}$ for charged lepton case. The effective Wilson coefficient $C_9^{\rm eff}$ including both the SD and long distance (LD) effects is [12]:

$$
C_9^{\rm eff}(s)=C_9+Y_{SD}(s)+Y_{LD}(s). \tag{25}
$$

The LD effect contributions are due to the J/ψ family. The explicit expressions of the $Y_{SD}(s)$ and $Y_{LD}(s)$ can be found in [12] (see also [17]). Table III also includes a comparison between our results and predictions of the other approaches including the LFQM, CQM and other methods [9]. Note that, the results presented as [9] are not the results directly obtained by analysis of the $B_s\to\eta(\eta')$, but they have been found relating the form factors of $B_s\to\eta_s$ to the form factors of $B\to K$ using the quark flavor scheme (see [9]). Hence,

the comparison of our results with the predictions of [9] is an approximate and for the exact comparison, the form factors should be directly available. In this Table, the set A refers to the values computed using short-distance QCD sum rules, set B shows the results obtained by light-cone QCD sum rules and set C corresponds to the results calculated via light-cone QCD sum rules within the Soft Collinear Effective Theory (SCET). From Table III, we see a good consistency in order of magnitude between our results and predictions of the other non-perturbative approaches. Here, we should also stress that the results obtained for the electron are very close to the results of the muon and for this reason, we only present the branching ratios for muon in our Tables.

In this part, we would like to present the branching ratios including LD effects. We introduce some cuts around the resonances of J/ψ and ψ' and study the following three regions for muon:

$$\begin{aligned} \mathrm{I}: \quad & \sqrt{q^2_{min}} \leq \sqrt{q^2} \leq M_{J/\psi} - 0.20, \\ \mathrm{II}: \quad & M_{J/\psi} + 0.04 \leq \sqrt{q^2} \leq M_{\psi'} - 0.10, \\ \mathrm{III}: \quad & M_{\psi'} + 0.02 \leq \sqrt{q^2} \leq m_{B_s} - m_P. \end{aligned} \tag{26}$$

and for tau:

$$\begin{aligned} \mathrm{I}: \quad & \sqrt{q^2_{min}} \leq \sqrt{q^2} \leq M_{\psi'} - 0.02, \\ \mathrm{II}: \quad & M_{\psi'} + 0.02 \leq \sqrt{q^2} \leq m_{B_s} - m_P. \end{aligned} \tag{27}$$

where $\sqrt{q^2_{min}} = 2m_l$. In Tables IV and V, we present the branching ratios for muon and tau obtained using the regions shown in Eqs. (26) and (27), respectively. The errors presented in Tables III, IV and V are due to uncertainties in determination of the auxiliary parameters, errors in input parameters, systematic errors in QCD sum rules as well as the errors associated to the following approximations used in the present work: a) the form factors are calculated in the low q^2 region and extrapolated to high q^2 using the fit parametrization in Eq. (22), b) the hadronic operators in the considered Hamiltonian can receive sizable non-factorizable corrections and the corresponding matrix elements may also be sensitive to the isosinglet content of the η and η' mesons. We show the dependency of the differential branching ratios on q^2 (with and without LD effects for charged lepton case) in Figs. (8)-(13).

Mode	I	II	III
$Br(B_s \to \eta\mu^+\mu^-)$	$(1.76 \pm 0.72) \times 10^{-7}$	$(2.20 \pm 0.90) \times 10^{-8}$	$(2.28 \pm 0.93) \times 10^{-8}$
$Br(B_s \to \eta'\mu^+\mu^-)$	$(1.81 \pm 0.74) \times 10^{-7}$	$(2.24 \pm 0.92) \times 10^{-8}$	$(1.32 \pm 0.54) \times 10^{-8}$

TABLE IV: The branching ratios of the semileptonic $B_s \to (\eta, \eta')\mu^+\mu^-$ decays including LD effects.

Mode	I	II
$Br(B_s \to \eta\tau^+\tau^-)$	$(0.40 \pm 0.16) \times 10^{-9}$	$(3.16 \pm 1.26) \times 10^{-8}$
$Br(B_s \to \eta'\tau^+\tau^-)$	$(0.43 \pm 0.17) \times 10^{-9}$	$(2.27 \pm 0.90) \times 10^{-8}$

TABLE V: The branching ratios of the semileptonic $B_s \to (\eta, \eta')\tau^+\tau^-$ decays including LD effects.

Finally, we want to calculate the longitudinal lepton polarization asymmetry for considered decays. It is given as [15]:

$$P_L = \frac{2v}{(1+\frac{2\hat{l}}{\hat{s}})\phi(1,\hat{r},\hat{s})\alpha_1 + 12\hat{l}\beta_1} \mathrm{Re}\left[\phi(1,\hat{r},\hat{s})\left(C_9^{eff} f_+(q^2) - \frac{2C_7 f_T(q^2)}{1+\sqrt{\hat{r}}}\right)(C_{10} f_+(q^2))^*\right], \tag{28}$$

where v, $\hat{l}$, $\hat{r}$, $\hat{s}$, $\phi(1,\hat{r},\hat{s}), \alpha_1$ and β_1 were defined before. The dependence of the longitudinal lepton polarization asymmetries for the $B_s \to (\eta, \eta')l^+l^-$ decays on the transferred momentum square q^2 with and without LD effects are plotted in Figs. 14 and 15.

As a result, the order of the obtained values for branching ratios as well as the longitudinal lepton polarization asymmetries show a possibility to study the considered transitions at LHC. Any experimental measurements on the presented quantities and those comparisons with the obtained results can give valuable information about the nature of the η and η' mesons and strong interactions inside them.

Acknowledgments

Partial support of Shiraz university research council is appreciated.

Appendix–A

In this appendix, the explicit expressions of the $\Pi_i^{non-per}$ are given,

$$\begin{aligned}
\Pi_+^{non-per}(p^2,p'^2,q^2) \;=\; \langle s\bar{s}\rangle\Bigg(& -\frac{m_s}{2rr'}+\frac{4m_0^2m_s-2m_0^2m_b+3m_s^3-3m_s^2m_b}{12rr'^2} \\
& +\frac{m_0^2m_b^3-m_0^2m_s^3+3m_s^4-3m_b^3m_s^2-2m_0^2m_b^2m_s+2m_0^2m_bm_s^2}{12r^2r'^2} \\
& +\frac{m_0^2m_sq^2-m_0^2m_bq^2+3m_b^2m_s^3-3m_bm_s^3+3m_bm_s^2q^2-3m_s^3q^2}{12r^2r'^2} \\
& +\frac{2m_0^2m_s-4m_0^2m_b+3m_sm_b^2-3m_s^2m_b}{12r^2r'} \\
& +\frac{m_0^2m_b^3-2m_b^3m_s^2+2m_b^2m_s^3-m_0^2m_b^2m_s}{4r^3r'} \\
& +\frac{2m_s^5-m_0^2m_s^3-2m_bm_s^4+m_0^2m_bm_s^2}{4rr'^3}\Bigg),
\end{aligned}$$

$$\begin{aligned}
\Pi_-^{non-per}(p^2,p'^2,q^2) \;=\; \langle s\bar{s}\rangle\Bigg(& \frac{2m_0^2m_b-9m_s^3+3m_s^2m_b}{12rr'^2} \\
& +\frac{3m_s^5-m_0^2m_b^3-m_0^2m_s^3+3m_b^3m_s^2+m_0^2m_bq^2+12m_0^2m_sq^2}{12r^2r'^2} \\
& +\frac{3m_b^2m_s^3+3m_bm_s^4-3m_bm_s^2q^2-3m_s^3q^2}{12r^2r'^2} \\
& +\frac{2m_0^2m_s-3m_sm_b^2+6m_s^2m_b-3m_s^2m_b}{12r^2r'} \\
& +\frac{2m_b^3m_s^2-m_0^2m_b^3+2m_b^2m_s^3-m_0^2m_b^2m_s}{4r^3r'} \\
& +\frac{2m_s^5-m_0^2m_s^3+2m_bm_s^4-m_0^2m_bm_s^2}{4rr'^3}\Bigg),
\end{aligned}$$

$$\begin{aligned}
\Pi_T^{non-per}(p^2,p'^2,q^2) \;=\; \langle s\bar{s}\rangle\Bigg(& \frac{2m_s^3+2m_sm_b+m_0^2}{4rr'} \\
& +\frac{3m_s^5-m_0^2m_b^2+3m_s^2q^2-m_0^2q^2+3m_s^4-6m_s^2m_b^2-m_sm_0^2m_b}{6rr'^2} \\
& +\frac{m_0^2m_b^4-m_0^2m_s^4+3m_s^6-3m_b^4m_s^2-m_0^2m_b^3m_s+m_0^2m_bm_s^3}{6r^2r'^2} \\
& +\frac{m_0^2m_s^2q^2-m_0^2m_b^2q^2+3m_b^2m_s^2q^2-3m_s^4q^2}{6r^2r'^2} \\
& +\frac{m_0^2m_s^2+3m_sm_b^3+m_0^2q^2-3m_s^2m_b^2+3m_s^4-3m_s^2q^2}{6r^2r'} \\
& +\frac{m_0^2m_bm_s-3m_s^3m_b}{6r^2r'}
\end{aligned}$$

$$+\frac{m_0^2 m_b^4 - 2m_b^4 m_s^2 + 2m_b^2 m_s^4 - m_0^2 m_b^2 m_s^2}{2r^3 r'}$$
$$+\frac{2m_s^6 - m_0^2 m_s^4 - 2m_b^2 m_s^4 + m_0^2 m_b^2 m_s^2}{2rr'^3}\Bigg),$$

where, $r = p^2 - m_b^2$ and $r' = p'^2 - m_s^2$.

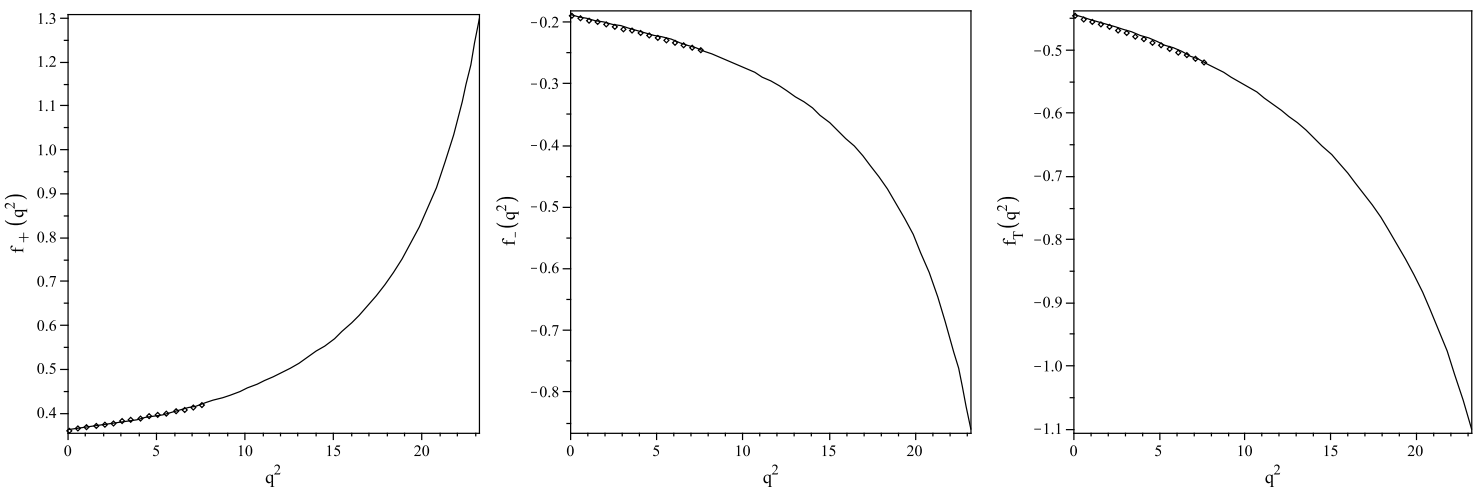

FIG. 6: The dependence of the form factors on q^2 at $M_1^2 = 12\ GeV^2$ and $M_2^2 = 5GeV^2$ for $P = \eta$. The small boxes correspond to the values obtained directly from sum rules and the solid lines belong to the fit parametrization of the form factors.

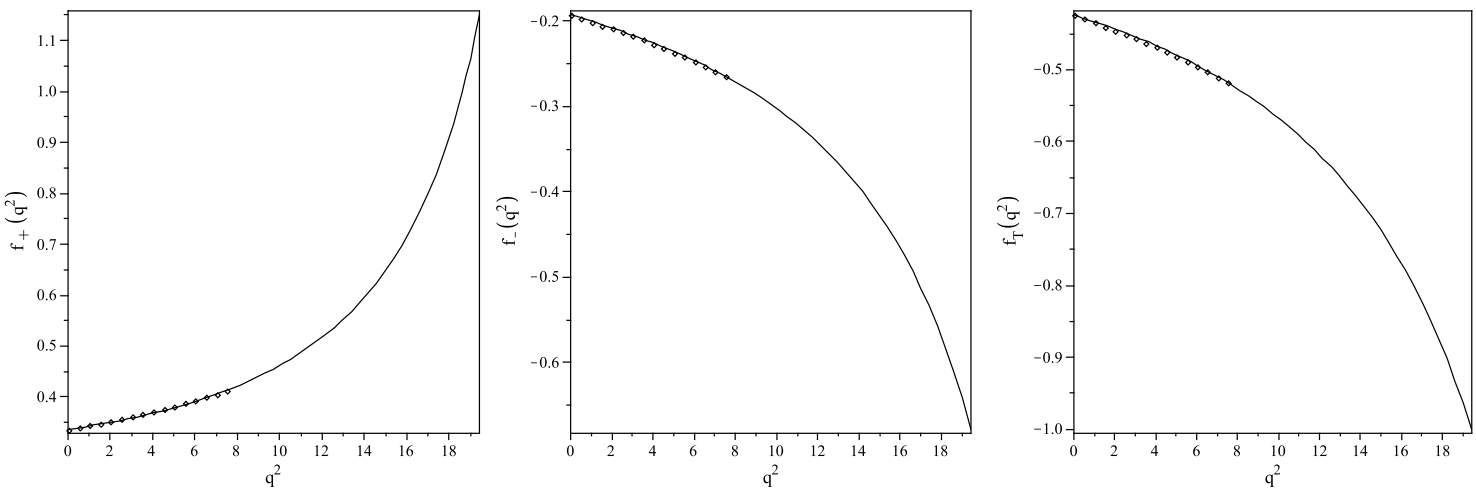

FIG. 7: The dependence of the form factors on q^2 at $M_1^2 = 12\ GeV^2$ and $M_2^2 = 5\ GeV^2$ for $P = \eta'$. The small boxes correspond to the values obtained directly from sum rules and the solid lines belong to the fit parametrization of the form factors.

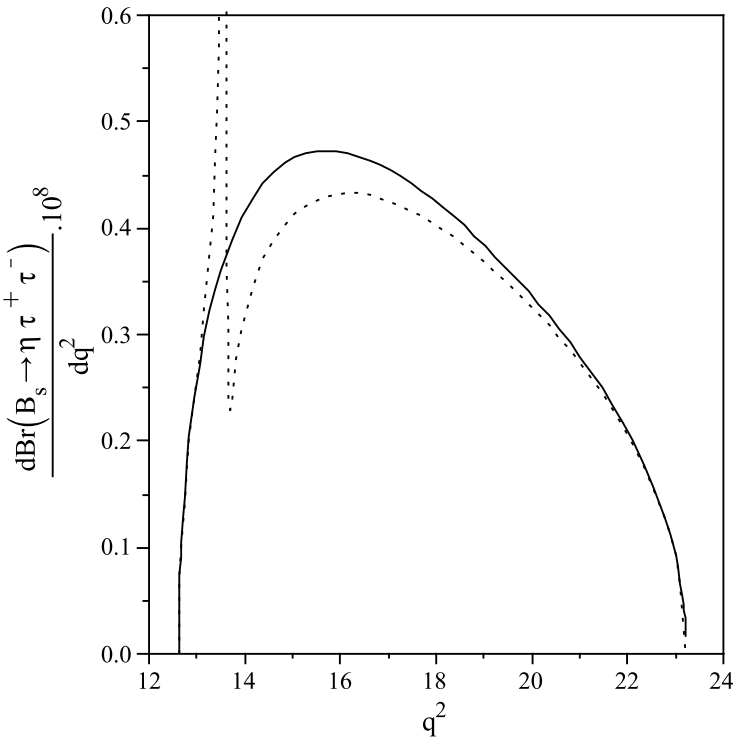

FIG. 8: The dependence of the differential branching fraction of the $B_s \to \eta\tau^+\tau^-$ decay with and without the LD effects on q^2. The solid and dotted lines show the results without and with the LD effects, respectively.

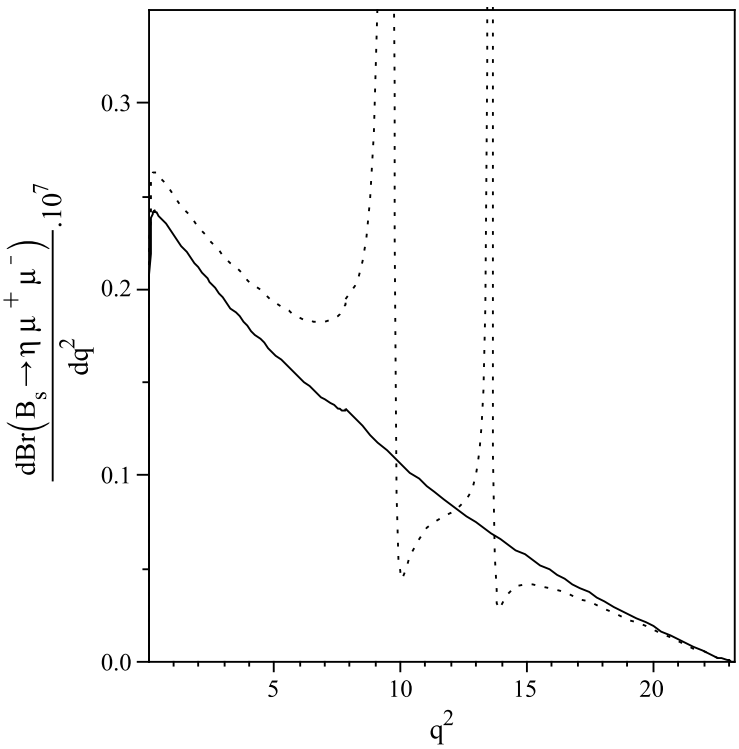

FIG. 9: The same as Fig 8 but for the $B_s \to \eta\mu^+\mu^-$.

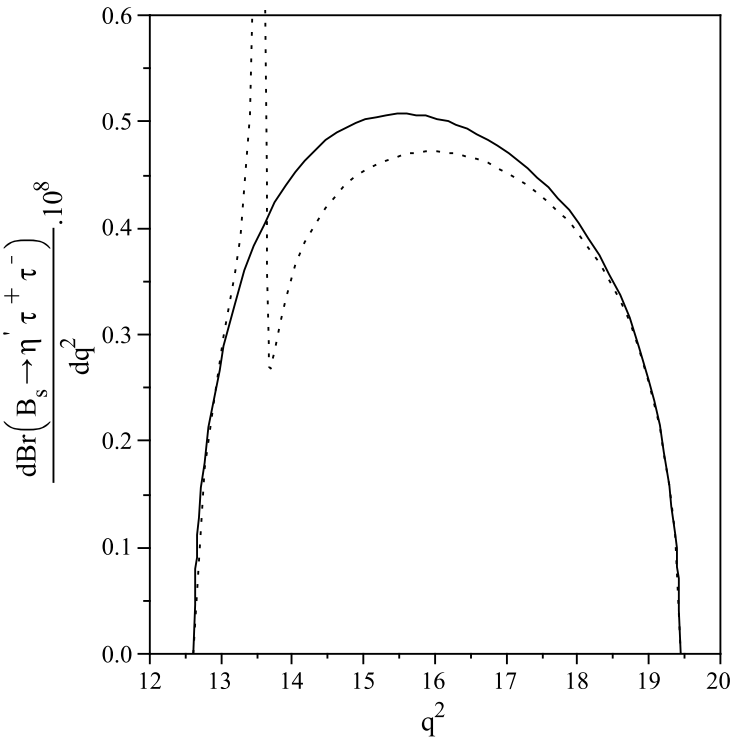

FIG. 10: The same as Fig 8 but for the $B_s \to \eta' \tau^+ \tau^-$.

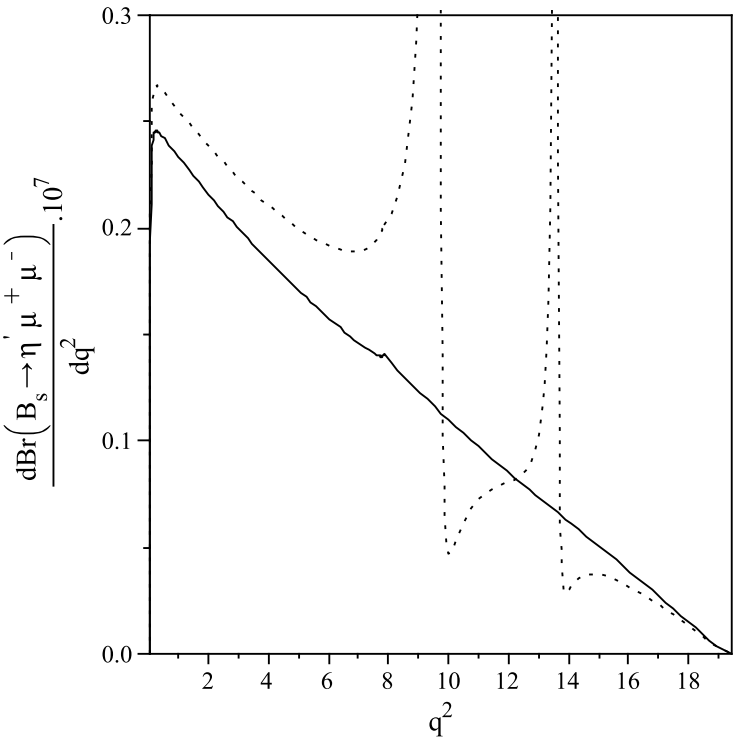

FIG. 11: The same as Fig 8 but for the $B_s \to \eta' \mu^+ \mu^-$.

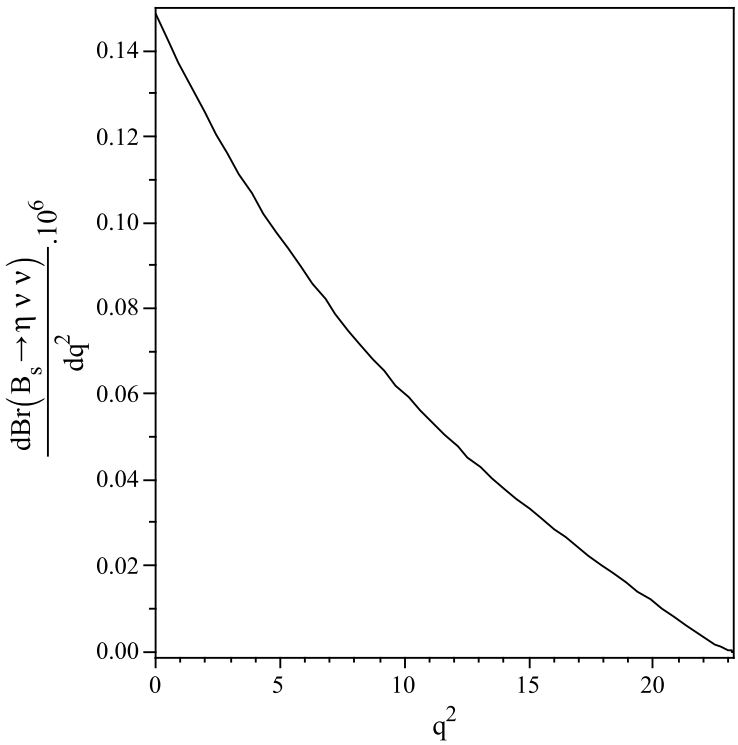

FIG. 12: The dependence of the differential branching fraction of the $B_s \to \eta\nu\bar{\nu}$ decay on q^2.

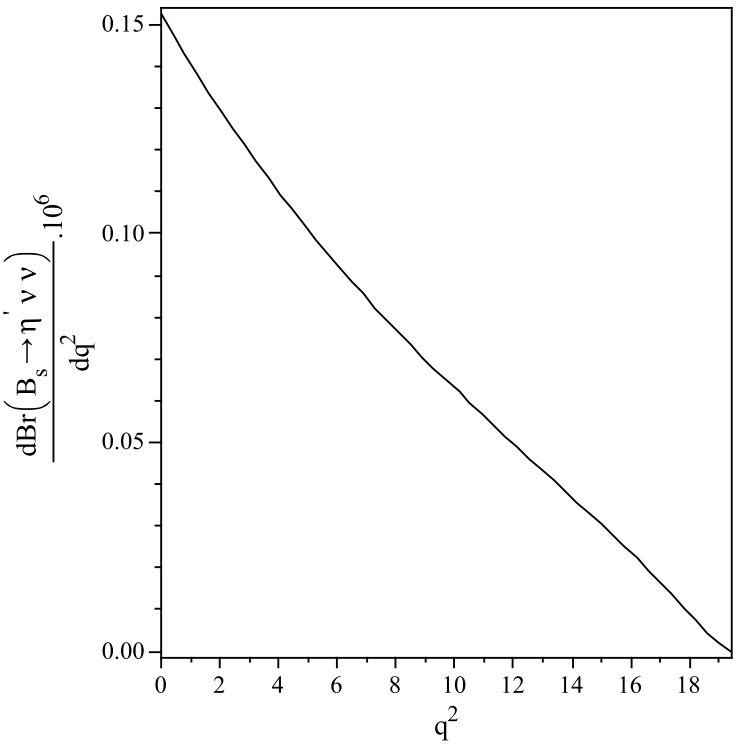

FIG. 13: The same as Fig 12 but for the $B_s \to \eta' \nu \bar{\nu}$.

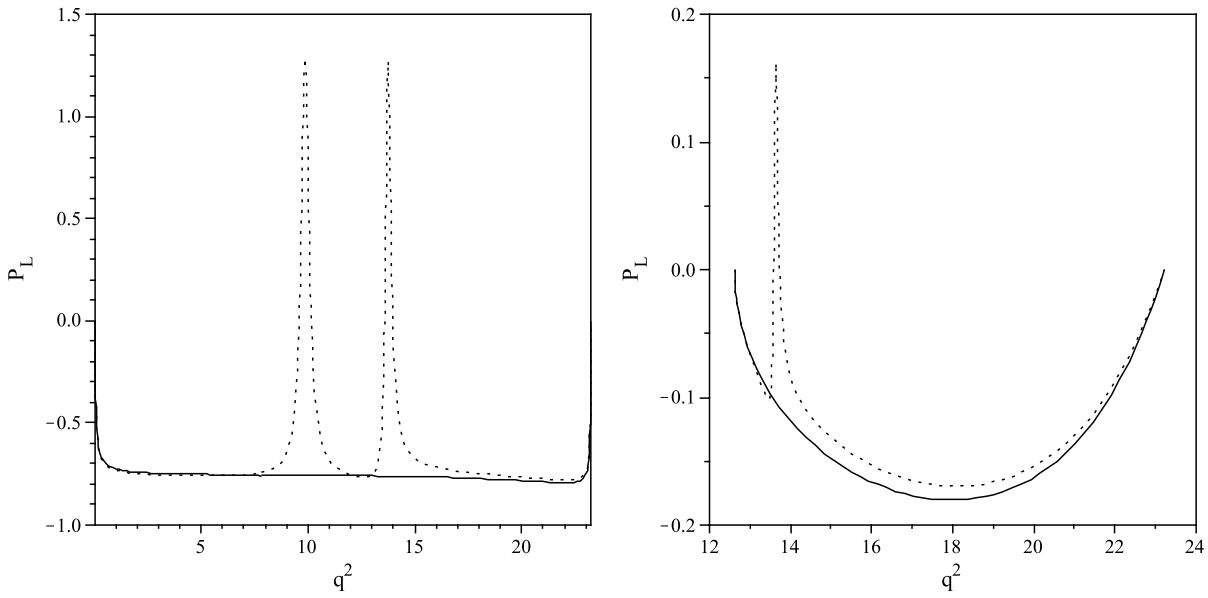

FIG. 14: The dependence of the Longitudinal lepton polarization asymmetry on q^2. The left figure belongs to the $B_s \to \eta\mu^+\mu^-$ decay and the right figure corresponds to the $B_s \to \eta\tau^+\tau^-$. The solid lines and dotted lines show the results without and with the LD effects, respectively.

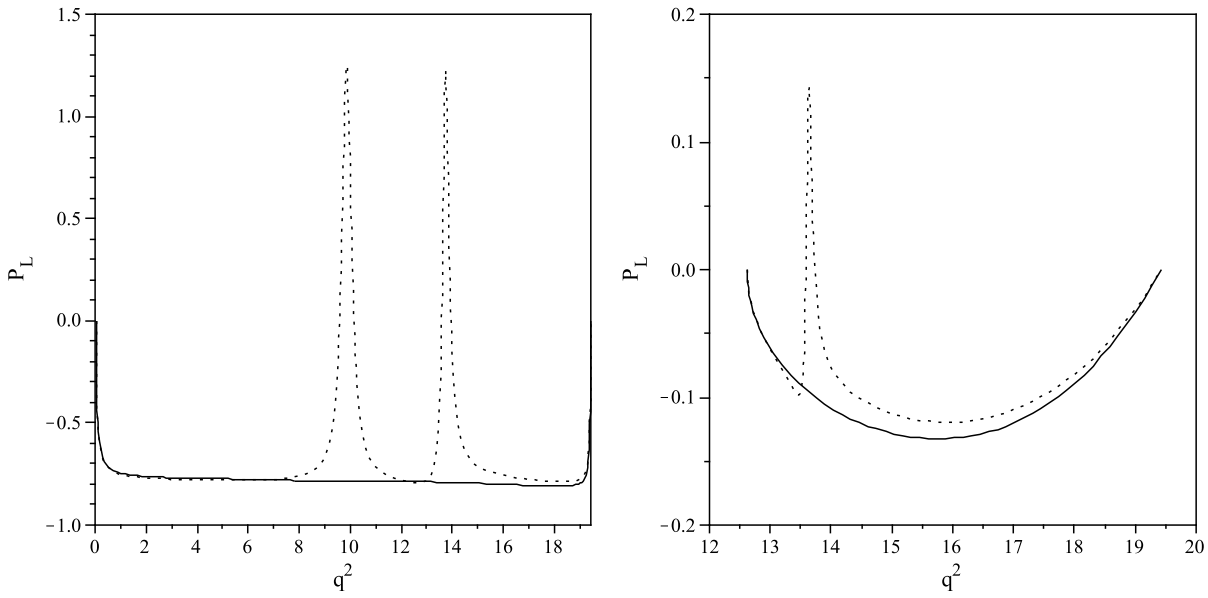

FIG. 15: The same as Fig 14 but for the $B_s \to \eta'$ transition.

[1] M. Artuso et al., (CLEO Collaboration), Phys. Rev. Lett. 95, 261801 (2005).

[2] G. Bonvicini et al., (CLEO Collaboration), Phys. Rev. Lett. 96, 022002 (2006).

[3] A. Drutskoy, arXiv:0905.2959 [hep-ex].

[4] G. Buchalla, G. Hiller, G. Isidori, Phys. Rev. D 63, 014015 (2000).

[5] C. Bird, P. Jackson, R. Kowalewski, M. Pospelov, Phys. Rev. Lett. 93, 201803 (2004).

[6] T. Feldmann, P. Kroll, B. Stech, Phys. Rev. D 58, 114006 (1998); Phys. Lett. B 449, 339 (1999); T. Feldmann, Int. J. Mod. Phys. A 15, 159 (2000).

[7] F. De Fazio, M. R. Pennington, JHEP 0007, 051 (2000).

[8] H. M. Choi, J. Phys. G 37, 085005 (2010).

[9] M. V. Carlucci, P. Colangelo, De. F. Fazio, Phys. Rev. D 80, 055023 (2009).

[10] F. Ambrosino et al. (KLOE Collaboration), Phys. Lett. B 648, 267 (2007).

[11] C. Amsler et al., Particle Data Group, Phys. Lett. B 667, 1 (2008).

[12] A. J. Buras, M. Muenz, Phys. Rev. D 52, 186 (1995).

[13] J. Rolf, M. Della Morte, S. Durr, J. Heitger, A. Juttner, H. Molke, A. Shindler, R. Sommer, Nucl. Phys. Proc. Suppl. 129, 322 (2004).

[14] P. Ball, R. Zwicky, Phys. Rev. D 71, 014015 (2005).

[15] C. H. Chen, C. Q. Geng, C. C. Lih, C. C. Liu, Phys. Rev. D 75, 074010 (2007).

[16] C. Q. Geng, C. C. Liu, J. Phys. G 29, 1103 (2003).

[17] A. Faessler, Th. Gutsche, M. A. Ivanov, J. G. Körner, V. E. Lyubovitskij, Eur. Phys. J. C 4, 18 (2002).